In Vivo Analysis of Trabecular Bone Architecture

W. J. Niessen[1], A. M. López[2], W. J. van Enk[1], P. M. v. Roermund[3]
B. M. ter Haar Romeny[1], M. A. Viergever[1]

[1] Image Sciences Institute, Utrecht University Hospital, Room E.01.334, Heidelberglaan 100, 3584 CX Utrecht, the Netherlands
[2] Computer Vision Center, Universitat Autònoma de Barcelona
[3] University Cluster of Orthopedics, Utrecht University Hospital

Abstract. Trabecular morphology has structural trends which are strongly correlated with physical function. In vivo analysis of the trabecular pattern has the potential to predict and treat malgrowth of bone owing to altered loading conditions in an early phase. Using multiscale texture analysis we determine the orientation trend of the trabecular network from CT images. First studies show that the obtained orientations in healthy individuals agree with histomorphometric studies. In vivo analysis of trabecular microstructure, to monitor development and progress of bone diseases as *e.g.* osteoporosis, is severely limited since high resolution CT and MR systems achieve at best resolutions in the order of the size of individual trabeculae.

1 Introduction

Bone structure and mass are strongly correlated with mechanical loading. External forces shape bone, while bone structure and mass determine bone strength. We propose in vivo analysis of trabecular morphology for two reasons. Firstly, external forces cannot be measured in vivo, therefore altered loading conditions are only apparent after the shape of the bone is affected. The orientation of the trabecular pattern gives insight in the main routes of stress. In vivo analysis of this pattern enables to predict changed loading conditions in an early phase to limit the extent of malgrowth. Secondly, bone diseases as *e.g.* osteoporosis become only relevant in the case of fracture. If the (often symptomless) underlying structural changes in trabecular morphology can be quantified, treatment can be started and monitored.

In section 2 we briefly describe trabecular bone morphology, and the relation of mechanical loading to the routes of stress. In section 3 we introduce the structure tensor which is applied to analyze oriented textures. It describes the local orientation by deriving an *angle* image which is supplied by a *confidence* estimate. Eigenvalue analysis of the structure tensor can also determine whether the local structure is platelike or rodlike. In section 4 we present results on 3D CT data.

2 Trabecular bone

Human bone can be classified as compact (cortical) or trabecular, depending on its relative density [7]. Most bones have both types, the compact part appears as a dense shell

of the bone, in contrast with the mesh appearance of the trabecular part, which covers the interior side of the shell. Bone is a living tissue that is continuously remodeled by actions of building cells (osteoblasts) and eroding cells (osteoclasts). Forces acting upon the bone play an important role in sculpting the internal structure and external shape.

Extensive histomorphometric studies, *e.g.* [3,18,7] have given considerable insight in trabecular bone structure. In healthy bone it consists of a connected network of platelike and rodlike elements, with a typical diameter of 100-300 μm and marrow spacings of 200-2000 μm. In order to visualize these structures in vivo, dedicated computed tomography methods are required [2,6,9,13]. However, the trabecular pattern is already visible at lower resolutions, which can be appreciated from conventional CT and MR images with a typical resolution of 1-4 mm^3.

As early as the end of the previous century relations between structural parameters and bone strength have been observed. According to the trajectory theory of Meyer and Culman [12]: "routes of stress coincide with trabecular patterns", while Wolff's law states that [19]: "the internal structure and external shape of a bone develop in response to the change in function and forces acting upon it". The routes of stress are artistically visualized for the ankle in Fig. 1 and for the femur in Fig. 2.

Some studies have already revealed relations between structure and mechanical loading. Gibson [7] showed that mechanical loading conditions influence trabecular geometry. Radiographic studies of the distal radius of children by Korstjens *et al.* [11] show that prevalence of trabeculae oriented perpendicular to the long axis of the radius decreases with age. Since the routes of stress appear at scales which are considerably higher than the individual trabeculae and vary within the human skeleton, we apply a multiscale texture analysis method based on the structure tensor [10,15,1].

A number of theoretical studies have fitted 3D models to the trabecular network in prepared specimens. Gibson [7] concludes that at low densities the trabecular network consists of rods while at larger densities the trabecular elements are platelike. Anisotropic loading conditions lead to anisotropic structures. Fazzalari *et al.* [4] consider surface to volume relations to conclude that the trabecular structure may consist of either a plate and rod network or a connected rod network. Osteoporosis appears to erode platelike trabecular structures and even remove plates and rods [14]. Since the structure tensor can determine whether the local structure is platelike or rodlike it enables a quantitative comparison over time.

3 Methods

Image analysis tools have been applied to obtain objective meaningful features of an oriented texture in 2D images [10,15] and, in general, n dimensional images [1,8]. In the case of oriented textures, the most meaningful features are the *angle image* and the *confidence image*, that together constitute the so-called *intrinsic images* of the textured image [15]. In our work we model the trabecular pattern as an oriented texture.

The angle image specifies the dominant orientation at each point. To compute this orientation, it is sufficient to analyze the behavior of the image gradient in a given neighborhood. We assume that, at a given point, there is a single dominant orientation

at most. Notice that the gradient of a function points into the direction of maximum change, and the dominant orientation is perpendicular to this direction. Two observations are crucial:

- The word *dominant* means dominant within a given neighborhood (window) of size σ_I centered at a given point $\mathbf{x} \in \mathbb{R}^n$, *i.e.* $\mathcal{W}(\mathbf{x}; \sigma_I)$. The parameter σ_I is known as integration scale.
- Since textured images are *views of a world scene* L, a measurement of L at $\mathbf{x}$ is necessarily performed using an operator of a certain size σ_D which is known as the differentiation scale.

To obtain derivatives of L in a well-posed fashion we use concepts of linear scale space theory. In this framework differentiation is defined as convolution with derivatives of Gaussians [5]:

$$\frac{\partial}{\partial x} L(\mathbf{x}; \sigma_D) = L(\mathbf{x}) * \frac{\partial}{\partial x} G(\mathbf{x}; \sigma_D) \tag{1}$$

where the n-dimensional Gaussian is defined as:

$$G(\mathbf{x}; \sigma) = \frac{1}{(2\pi\sigma^2)^{\frac{n}{2}}} \; e^{-\frac{\|\mathbf{x}\|^2}{2\sigma^2}} \tag{2}$$

For simplicity we first consider the 2-dimensional case. In this case the dominant orientation at each point of the image will be given by an angle in $[-\frac{\pi}{2}, \frac{\pi}{2})$ (we are interested in the orientation, not in the specific direction; opposite directions should be identified). This yields a 2-dimensional array of angles that we coin the *angle image*.

To summarize, the steps to compute the angle $\theta(\mathbf{x}; \sigma_I; \sigma_D)$ are:

i) compute the gradients $\nabla L(\mathbf{y}; \sigma_D) \; \forall \; \mathbf{y} \in \mathcal{W}(\mathbf{x}; \sigma_I)$.

ii) determine the dominant orientation of these gradients: $\alpha(\mathbf{x}; \sigma_I; \sigma_D)$ by averaging the squared vectors [10,15]:

$$2\alpha(\mathbf{x}; \sigma_I; \sigma_D) = \sum_{\mathbf{y} \in \mathcal{W}(\mathbf{x}; \sigma_I)} w_{\mathbf{y}} l_{\mathbf{y}}^2 e^{\imath 2\theta_{\mathbf{y}}} \tag{3}$$

where $w_{\mathbf{y}}$ is a weighting factor, $l_{\mathbf{y}} = \|\nabla L(\mathbf{y}; \sigma_D)\|$, and $\theta_{\mathbf{y}}$ denotes the angle between the X-axis and the gradient direction.

iii) determine the dominant direction, which is perpendicular to the dominant gradient orientation.

This reasoning is equivalent [8] to the eigenvalue analysis of the so-called *structure tensor*, which generalizes to n dimensions. The structure tensor can be represented by means of a symmetric and semi-positive definite $n \times n$ matrix

$$\mathbf{M}(\mathbf{x}; \sigma_I; \sigma_D) = \mathcal{W}(\mathbf{x}; \sigma_I) * (\nabla L(\mathbf{x}; \sigma_D) \nabla L(\mathbf{x}; \sigma_D)^T) \tag{4}$$

where $\mathcal{W}(\mathbf{x}; \sigma_I)$ is convolved elementwise with the matrix. A suitable choice for the window is a Gaussian profile, *i.e.* $\mathcal{W}(\mathbf{x}; \sigma_I) = G(\mathbf{x}; \sigma_I)$. This choice implies that neighbors are weighted as a function of their distance.

The orientation $\alpha(\mathbf{x};\sigma_I;\sigma_D)$ of step *ii)* above is given by the eigenvector which corresponds to the highest eigenvalue of $\mathbf{M}(\mathbf{x};\sigma_I;\sigma_D)$. However, we have assumed that every point has a preferred orientation. To check this assumption we introduce a confidence (or coherence) measure to a given orientation; we associate a value $\mathcal{C}(\mathbf{x};\sigma_I;\sigma_D) \in [0,1]$ to the angle $\theta(\mathbf{x};\sigma_I;\sigma_D)$, which can be computed from the eigenvalues of the structure tensor [1,8]. In the two dimensional case, for example, similarity of the two eigenvalues of the structure tensor implies isotropy and, as a result $\mathcal{C}(\mathbf{x};\sigma_I;\sigma_D)$ should be close to zero. A logical choice is a measure which checks whether the difference in eigenvalues ($\lambda_\triangle$) exceeds a predefined threshold c, which is characteristic for $\lambda_\triangle$ in the trabecular pattern: $\mathcal{C} = 1 - e^{-\frac{(\lambda_\triangle)^2}{2c^2}}$.

Eigenvalue analysis of the structure tensor also gives insight in the local structure. Rodlike structures yield two large and one small eigenvalue, while platelike structures yield one large and two small eigenvalues.

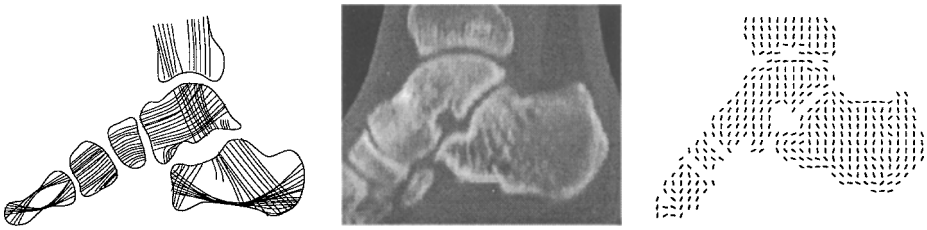

Fig. 1. Left: Redrawn version of D'Arcy Thompson's [17] diagram of the stress lines in the human foot. The sketched orientations have been confirmed by histomorphometric studies. **Middle**: High resolution sagittal CT slice of the ankle. Resolution = 425 × 425 μm. Slice thickness is 1 mm. **Right**: Trabecular orientation for $\sigma_I = 4$ and $\sigma_D = 0.5$ pixels.

4 Results

In Fig. 1 we plot the sagittal component of the orientation of the trabecular pattern for an in vivo ankle CT image. In the tibia the orientations agree very well. In Fig. 2 we plot the coronal component of the orientation of the trabecular pattern at two integration scales for the femur CT image. Since in large parts the orientation is not very accurately known we used the confidence image to select only the vectors for which $\mathcal{C} > 0.5$, where c has been selected upon inspecting the trabecular pattern in the femoral neck. Cortical bone has significant influence on the estimation of the trabecular orientation, especially for higher scales. The orientation in the femoral neck corresponds qualitatively with the orientations in the artistic impression.

In Fig. 2 we plot the regions in which the pattern is rodlike and platelike. Note, however, that the resolution of the images is insufficient to quantify the shape of individual trabeculae.

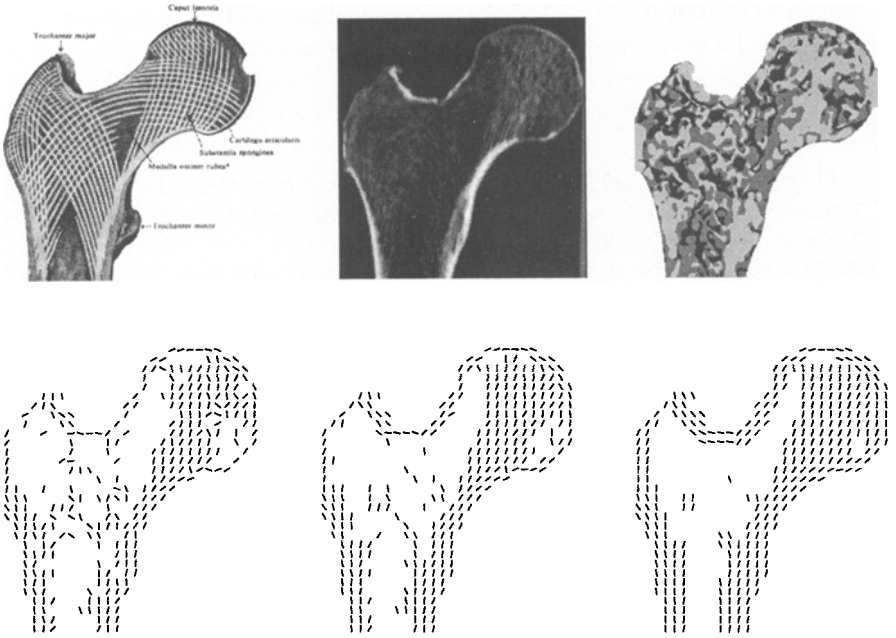

Fig. 2. Top row left: An artistic impression of the stress trajectories based on the orientation field observed in the trabecular patterns in the head of the femur. Reproduced from [16] with permission from the publisher. **Top row middle**: CT slice of dry femur. Resolution = 245× 245 μm. Slice thickness is 0.5 mm. **Top row right**: Upon inspecting the relative eigenvalues, platelike (one high eigenvalue; dark area) and rodlike (two high eigenvalues; bright area) regions can be identified. The grey area represents either a smooth (all eigenvalues are small) or noisy (all eigenvalues are large) region. Note that all these measures are relative, but they can be useful in follow-up studies. **Bottom row**: Trabecular orientation for three different integration scales. We used $\sigma_I = 2$ (left), $\sigma_I = 4$ (middle), and $\sigma_I = 8$ (right) respectively, while $\sigma_D = 0.5$ pixels. Vectors are plotted for which the confidence $C > 0.5$; $c = 1000$ Hounsfield units.

5 Discussion

We have presented the feasibility of in vivo studies of the trabecular orientation pattern. CT studies show strong correlation between the obtained orientations and data from histomorphometric studies. This shows the potential to detect altered loading conditions in an early phase, so treatment can be started to limit the extent of malgrowth.

A drawback of the presented method is that at one location only a single preferred orientation is present. We are currently considering texture autocorrelation to study multiple preferred orientations. However, these methods are more expensive from a computational point of view.

The presented method is also capable of analyzing the local architecture. However, to quantify structural changes at the level of individual trabeculae in *e.g.* osteoporosis

resolutions of at least $100 \times 100 \times 100\ \mu m$ are required. An MR study on the finger [9] shows that for the extremities these resolutions become in reach.

References

1. J. Bigun, G. Granlund, and J. Wiklund. Multidimensional orientation estimation with applications to texture analysis and optical flow. *IEEE Transactions on Pattern Recognition and Machine Intelligence*, 13(8):775–790, 1991.
2. E. P. Durand and P. Rüegsegger. Cancellous bone structure: Analysis of high resolution CT images with the run length method. *Journal of Computer Assisted Tomography*, 15(1):133–139, 1991.
3. E. D. Dyson, C. K. Jackson, and W. J. Whitehouse. Scanning electron microscope studies of human trabecular bone. *Nature*, 225:957–959, 1970.
4. N. J. Fazzalari, D.J Crisp, and B. Vernon-Roberts. Mathematical modeling of trabecular bone structure: the evaluation of analytical and quantified surface to volume relationships in femoral head and iliac crest. *Journal of Biomechanics*, 22(8):901–910, 1989.
5. L. M. J. Florack, B. M. ter Haar Romeny, J. J. Koenderink, and M. A. Viergever. Scale and the differential structure of images. *Image and Vision Computing*, 10(6):376–388, 1992.
6. T. K. F. Foo, F. G. Shellock, C. E. Hayes, J. F. Schenck, and B. E. Slayman. High-resolution MR imaging of the wrist and eye with short TR, short TE, and partial echo acquisition. *Radiology*, 183(1):277–281, 1992.
7. L. J. Gibson. Mechanical behavior of cancellous bone. *Journal of Biomechanics*, 18(5):317–328, 1985.
8. B. Jähne. *Spatio-Temporal Image Processing*. Lecture Notes in Computer Science 751. Springer Verlag, Berlin-Heidelberg, 1993.
9. H. Jara, F. W. Wehrli, H. Chung, and J. C. Ford. High-resolution variable flip angle 3D MR imaging of trabecular microstructure in vivo. *Magnetic Resonance in Medicine*, 29:528–539, 1993.
10. M. Kass and A. Witkin. Analyzing oriented patterns. *Computer Vision, Graphics, and Image Processing*, 37:362–385, 1987.
11. C. M. Korstjens, W. G. M. Geraets, F. C. van Ginkel, B. Prahl-Andersen, P. F. van der Stelt, and A. H. Burger. An analysis of the orientation of the radiographic trabecular pattern in the distal radius of children. *Growth, Development and Aging*, 58(4):211–221, 1994.
12. H. Meyer and M. Culman. Die architektur der spongiosa. *Arch. Anat. Physiol.*, 47(1):615–628, 1867.
13. R. Müller and P. Rüegsegger. Three dimensional finite element modeling of non-invasively assessed trabecular bone structures. *Journal of Medical Engineering Physics*, 17:126–133, 1995.
14. A. M. Parfitt. Trabecular bone architecture in the pathogenesis and prevention of fracture. *American Journal of Medicine*, 82:68–72, 1987.
15. A. R. Rao and B. Schunck. Computing oriented texture fields. *Graphical Models and Image Processing*, 53(2):157–185, 1991.
16. W. Spalteholz. *Atlas of Human Anatomy*. Scheltema & Holkema NV, Amsterdam, 1967. 16th edition, revised by R. Spanner.
17. D. W. Thompson. *On Growth and Form: abridged edition*. Cambridge University Press, London, 1917. ed. J. T. Bonner, 1961.
18. W. J. Whitehouse. The quantitative morphology af anisotropic bone. *Journal of Microscopy*, 101:153–168, 1974.
19. J. Wolff. Ueber die innere architektur der knochen. *Virchow's Arch.*, 50(1):389–453, 1870.